

PILOT PROCESSING OF 18.6% EFFICIENT REAR SURFACE PASSIVATED SILICON SOLAR CELLS WITH SCREEN PRINTED FRONT CONTACTS

A. Wolf¹, E. A. Wotke¹, S. Mack¹, J. Nekarda¹, D. Biro¹, R. Preu¹, K. Schlegel², T. Weber², J. Lossen³, T. Böske³, A. Grohe³, P. Engelhart⁴, J. W. Müller⁴, G. Schubert⁵, H. Plagwitz⁵ and Y. Gassenbauer⁶

¹Fraunhofer Institute for Solar Energy Systems (ISE), Heidenhofstr. 2, D-79110 Freiburg, Germany

Tel: +49-761-4588-5580, Fax: +49-761-4588-9250, andreas.wolf@ise.fraunhofer.de

²SolarWorld Innovations GmbH, Berthelsdorfer Str. 111A, D-09599 Freiberg, Germany

³Bosch Solar Energy AG, Wilhelm-Wolff-Str. 23, D-99099 Erfurt, Germany

⁴Q-Cells SE, Sonnenallee 17-21, D-06766 Bitterfeld-Wolfen, Germany

⁵Sunways AG, Macairestr. 3-5, D-78467 Konstanz, Germany

⁶SCHOTT Solar AG, Carl-Zeiss-Str. 4, D-63755 Alzenau, Germany

ABSTRACT: We apply the recently introduced Silicon Nitride Thermal Oxidation (SiNTO) process for the industrial fabrication of silicon solar cells that feature a thermal oxide-passivated rear surface. The SiNTO process utilises a SiN_x anti-reflection layer for masking the front side of the solar cell during the thermal oxidation process. This masking layer limits the growth of the thermal oxide to the uncoated rear surface. Laser fired contact (LFC) technology is applied to form the local rear contacts. An efficiency of 18.6% (annealed) and 18.4% (stable, independently confirmed) is achieved for a PERC device fabricated from boron-doped Czochralski-silicon by means of the SiNTO process. The average efficiency of a batch of 34 SiNTO cells is 18.2%, measured after fabrication (not stabilised). Parallel processed Al-BSF references reach average efficiencies of 17.7%. Thus, the SiNTO approach enables an efficiency increase of 0.5% absolute compared to conventional Al-BSF technology. When introducing soldering pads, the efficiency gain for SiNTO compared to Al-BSF cells even increases to 0.8% absolute. Finally, we use a comprehensive analytical model to estimate the optimum bulk resistivity for locally contacted devices fabricated from conventional Czochralski silicon material. These calculations account for the bulk recombination caused by the formation of boron-oxygen complexes under carrier injection.

Keywords: thermal oxide, surface passivation, local contacts

1 INTRODUCTION

Industrial silicon solar cells of current production status exhibit a high rear surface recombination and a poor internal reflection of the full area Al back surface field (BSF). The passivated rear surface of a passivated emitter and rear cell (PERC) [1] combines low surface recombination with a high internal reflection. This concept enables significantly higher efficiencies compared to the Al-BSF technology [2]. Thermally grown oxides permit excellent and stable surface passivation and were used to fabricate highly efficient silicon solar cells [3]. Thermal oxidation is a proven industrial process available at competitive cost [4]. The recently introduced Silicon Nitride Thermal Oxidation (SiNTO) process [5] enables the industrial fabrication of silicon solar cells that feature an oxide-passivated rear surface, thereby maintaining the front end part from the conventional Al-BSF fabrication process.

2 FABRICATION PROCESS AND DEVICE STRUCTURE

Silicon solar cells of PERC design are fabricated from conventionally pulled boron-doped 3 Ωcm Czochralski (Cz) silicon using the SiNTO approach. In addition, conventional Aluminium back surface field (Al-BSF) solar cells are fabricated to enable an evaluation of the efficiency potential of the SiNTO process with respect to parallel processed solar cells of current production status. Figure 1 presents the process flow. Each of the two routes contains solar cells with and

without soldering pads. The frontend processing is carried out in an industrial production line at Deutsche Cell GmbH, Freiberg, Germany, whereas passivation and backend processing is performed at Fraunhofer ISE Photovoltaic Technology Evaluation Center (PV-TEC) [6]. The production line process sequence starts with an alkaline texture to remove the saw damage and form a random pyramid surface structure. In the next step, a tube furnace diffusion using POCl₃ as precursor gas forms a phosphorus-doped emitter. After removing the phosphosilicate glass (PSG), a SiN_x anti reflection layer is deposited onto the front surface. From here on, processing is performed at PV-TEC pilot line. First, wet chemical etching removes the emitter from the rear surface. During this process the SiN_x layer serves as a mask to protect the front emitter from being etched.

In case of the PERC devices (Groups 1 and 2), a wet chemical cleaning sequence follows and a ~10 nm thick thermal oxide is grown in a tube furnace using a water vapour atmosphere. In the next step, we deposit a SiO_x capping layer onto the rear surface by plasma enhanced chemical vapour deposition (PECVD). This capping layer prevents spiking of the subsequently evaporated Al layer and ensures a high internal reflectivity. Screen printing then forms the 4 mm wide Ag-Al soldering pads (only Group 2) and the Ag front contact grid, followed by firing in a conveyor belt furnace for contact formation. The rear contact consists of a 2 μm thick layer of aluminium deposited by electron beam (e-gun) evaporation. For the samples from Group 2, masking prevents the complete coverage of the soldering pads by the Al layer. A laser then alloys the local rear contacts

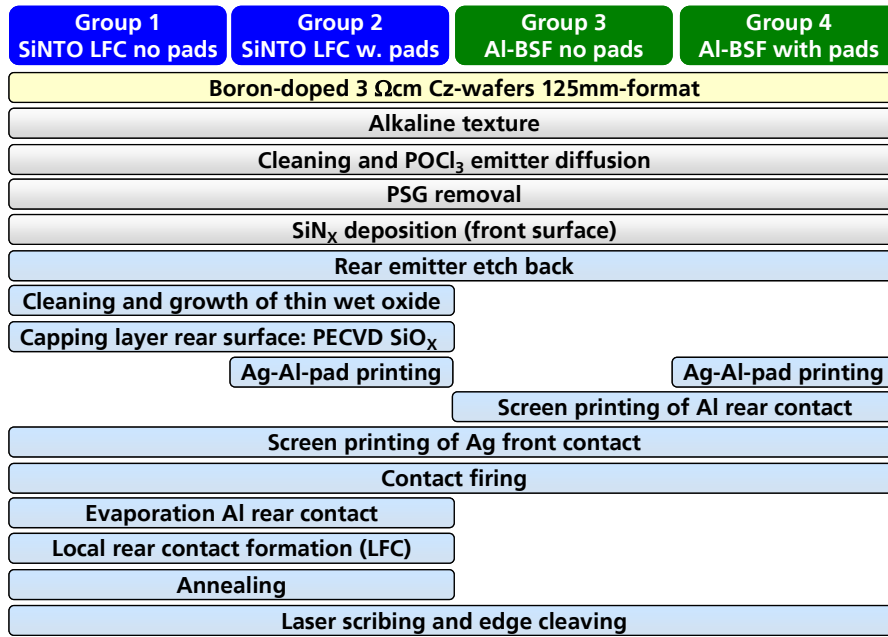


Figure 1: Process sequence for the fabrication of PERC structures using the SiNTO approach (Groups 1 and 2) and a conventional Al-BSF process (Groups 3 and 4). Each of the two routes contains solar cells with (Groups 2 and 4) and without (Groups 1 and 3) soldering pads. The top four process steps (gray coloured bars) are carried out in a production line at Deutsche Cell GmbH, Freiberg, Germany. The subsequent steps (light blue coloured bars) are processed at Fraunhofer ISE PV-TEC pilot line.

through the dielectric layers (laser fired contacts, LFC) [7]. Finally, the samples are annealed in forming gas at a temperature of 350 °C for 5 minutes. Due to the geometry of the sample holder, the Al rear contact does not cover the whole rear surface of the cell. To evaluate the potential of a full area rear contact, the cells are scribed by a laser and subsequently cleaved removing about 3 mm of the wafer edge. The resulting cell area is 136 cm². Figure 2 schematically illustrates the SiNTO LFC device structure.

For the Al-BSF solar cells (Groups 3 and 4), after the rear emitter etch, the soldering pads (only Group 4) and the full area Al layer are screen printed onto the rear surface, followed by screen printing of the front contacts and contact firing. The annealing step is not performed but the Al-BSF cells do receive edge cleaving to ensure similar size and edge geometry as the SiNTO cells.

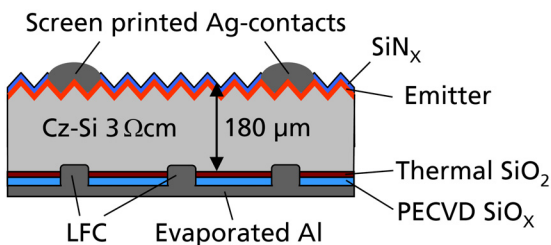


Figure 2: Schematic of the PERC device fabricated using the SiNTO approach (Group 1). The rear surface passivation consists of a thin thermal oxide covered by a SiO_x capping layer deposited by PECVD. Conventional screen printing is used for the formation of the front contacts.

3 RESULTS AND DISCUSSION

Figure 3 shows the efficiency distribution for a batch of 34 SiNTO LFC solar cells (Group 1) which have been fabricated with the above described process sequence. The illuminated current-voltage (IV) measurements are performed after the fabrication process using an industrial cell tester equipped with a flash lamp. Please note that the cells are not stabilised prior to the measurements. For comparison, the distribution for a batch of Al-BSF cells (Group 3) is shown as well. For the SiNTO LFC devices from Group 1, an average efficiency of 18.2% is achieved. The increase in efficiency compared to the Al-BSF references from Group 3 is 0.5% absolute. The average efficiency for the SiNTO cells from Group 2 is 18.1% whereas the Al-BSF cells from Group 4 reach an average of 17.3% (both not shown). Thus, when introducing soldering pads, the efficiency gain for SiNTO compared to Al-BSF cells even increases to 0.8% absolute.

Table I lists the IV-parameters measured for the best cell from each group. The measurements are performed at Fraunhofer ISE CaLab PV Cells under the IEC standard IEC60904-3Ed.2 (2008). Prior to the measurements, illumination for 36 hours at ~1 sun stabilises the devices. For the best cell from Group 1, a second measurement is performed after subsequent hotplate annealing. A stable efficiency of 18.4% is reached for the best SiNTO LFC cell from Group 1, the annealed device achieves 18.6%. Again, an efficiency gain of more than 0.5% (without pads) and 0.8% (with pads) absolute is visible for the SiNTO LFC devices compared to the corresponding Al-BSF reference. The passivated rear surface yields an increase in the short circuit current density J_{SC} of ~1 mA/cm² and a ~10 mV higher open circuit voltage V_{OC} . This advantage results

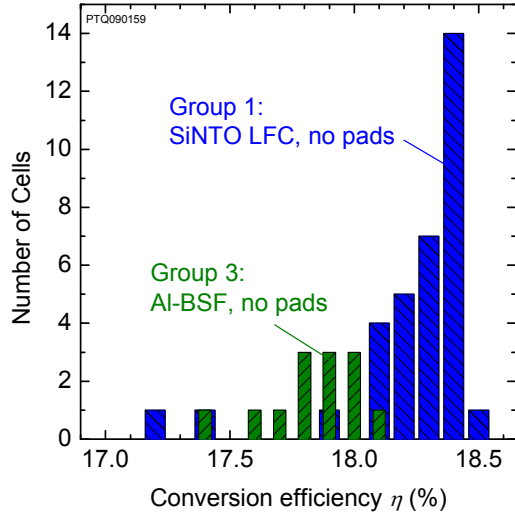


Figure 3: Efficiency distribution measured for a batch of 34 SiNTO LFC solar cells (Group 1). For comparison, the distribution for a batch of Al-BSF cells (Group 3) is shown as well. All cells feature cleaved edges and no soldering pads. The cell area is 136 cm². The cells are not stabilised before the IV measurement.

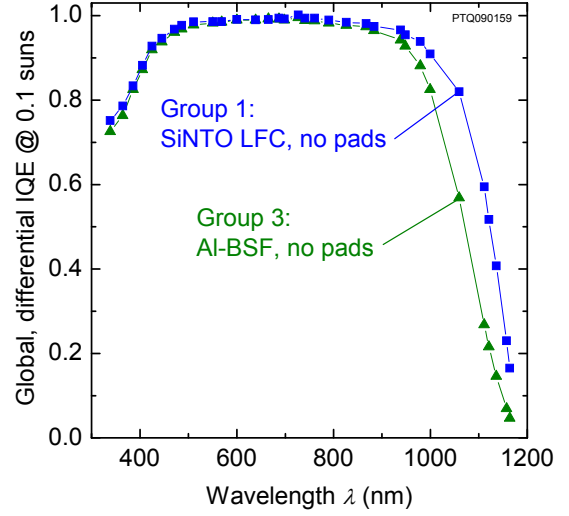


Figure 4: Global, differential IQE of a SiNTO LFC device (Group 1) and an Al-BSF reference (Group 3) measured at a bias illumination of 0.1 suns. Prior to the measurement the cells are stabilised by 1 sun illumination for 36 hours.

from an increased internal reflection and a reduced surface recombination velocity which overcompensate the lower fill factor FF caused by current crowding at the local contacts.

For both structures the introduction of soldering pads decreases V_{OC} by ~ 10 mV due to increased surface recombination at the pad area where no highly doped BSF is present. It seems that in case of the PERC devices, the Ag-Al pad paste fires through the passivation layer or at least damages the passivation. Moreover, the fill factor of the PERC devices increases by $\sim 1\%$ absolute when introducing soldering pads. It seems that the increased contact area reduces the series resistance, however this effect is still investigated. Please note that in this work quite large pad areas, namely ~ 4 mm wide stripes from edge to edge, are applied. The pads cover $\sim 7\%$ of the rear surface.

Recent results showed that an innovative module interconnection technology enables the fabrication of modules from SiNTO LFC solar cells that did not feature soldering pads [8]. On the other hand, soldering pads that

do not fire through the passivation layer represent another approach to maintain high open circuit voltages in the finished module. The use of screen printed instead of evaporated Al rear contacts allows the fabrication of fully screen printed PERC devices [9]. Small area high efficiency solar cells with screen printed Al rear metallisation and LFCs already showed efficiencies of up to 21.2% [10].

In this work, laser scribing and edge cleaving is used for all cells. However, due to a process adaption, in a recent experiment we were able to fabricate SiNTO LFC solar cells of 156 mm format that achieved fill factors of up to 77.9% without the use of any edge treatment [8].

Figure 4 presents the global, differential internal quantum efficiency (IQE) measured for a stabilised cell from Group 1 and 3. The increased red response of the PERC structure compared to the Al-BSF cell is clearly visible. A quantitative analysis of the IQE [11] yields an effective diffusion length of ~ 600 μm for the Al-BSF structure and ~ 1000 μm for the SiNTO LFC cell, which confirms the superior rear surface passivation of the latter.

Table I: Parameters measured for the best cell from each group. The state “stabilised” denotes a measurement performed after 1 sun illumination for 36 hours, “annealed” refers to a measurement directly after annealing at 200 °C for 20 minutes. The measurements are independently confirmed by Fraunhofer ISE CalLab PV Cells under the IEC standard IEC60904-3Ed.2 (2008). The cell area is 136 cm², the cells feature cleaved edges.

Group	Type	Pads	State	V_{OC} (mV)	J_{SC} (mA/cm ²)	FF (%)	η (%)
1	SiNTO LFC	No	annealed	631	37.9	78.0	18.6
1	SiNTO LFC	No	stabilised	630	37.6	77.6	18.4
2	SiNTO LFC	Yes	stabilised	619	37.3	78.6	18.1
3	Al-BSF	No	stabilised	619	36.6	78.7	17.8
4	Al-BSF	Yes	stabilised	609	36.0	78.9	17.3

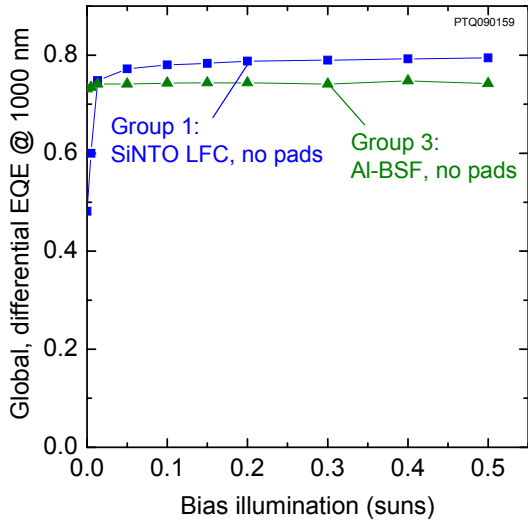


Figure 5: Bias illumination dependence of the global, differential EQE of a SiNTO LFC device (Group 1) and an Al-BSF reference (Group 3) measured at a wavelength of 1000 nm. Prior to the measurement the cells are stabilised by illumination for 36 hours

Figure 5 illustrates the dependence of the global, differential external quantum efficiency (EQE) at a wavelength of 1000 nm on the bias illumination level for both cell types. Apparently, for the Al-BSF device the bias illumination hardly affects the EQE, since the recombination at the BSF high-low junction does not exhibit a strong dependence on injection level [12]. In contrast, the surface recombination velocity (SRV) at thermal oxide passivated silicon surfaces shows a significant injection dependence due to fixed positive surface charges and asymmetric capture cross sections [13-15]. Moreover, the interaction of the local contacts with a possible inversion layer, induced by the positive fixed surface charges, would reduce J_{SC} and lead to a bias-dependence of the EQE as well [16,17]. However, for the SiNTO LFC cell the impact of these effects seem to be limited to very low intensities below 0.02 suns (see Fig. 5), which is of minor relevance for out-door operation. For higher bias illumination levels, the EQE of the SiNTO device exceeds that of the Al-BSF reference and saturates at that higher level for illumination intensities above ~ 0.05 suns.

4 OPTIMUM BASE DOPING LEVEL

Locally contacted devices benefit from a high base doping concentration since ohmic losses due to current crowding at the local contacts are reduced. However, for conventionally pulled Czochralski silicon material, carrier injection facilitates the formation of recombination-active boron-oxygen complexes, which reduces the bulk diffusion length [18-20]. The defect concentration scales with the boron concentration, thus low resistivity material typically shows bulk lifetimes way below the Auger lifetime limit. Consequently, for optimum performance, resistance and bulk recombination losses have to be balanced.

We recently introduced a comprehensive analytical model for locally contacted solar cells. Details of the model are presented in a different publication [21]. Our model accounts for ohmic losses and rear surface, emitter, and bulk recombination. Moreover, we include the device optics yielding a complete analytic description of the device [22]. Here, we use the model to estimate the optimum bulk doping level for thermal oxide passivated LFC PERC solar cells fabricated from conventional boron-doped Cz silicon material. This calculation involves several material and device parameters. All details are described in Ref. [21], here we briefly recapitulate the most important parameters.

Bothe *et al.* introduced a parameterisation for the boron-oxygen complex recombination limited bulk carrier lifetime [23]

$$\frac{\tau_{B-O}}{1\mu s} = 2 \times 7.675 \times 10^{45} \times \left(\frac{N_A}{1\text{cm}^{-3}} \right)^{0.824} \times \left(\frac{[O_i]}{1\text{cm}^{-3}} \right)^{1.748}, \quad (1)$$

where N_A is the doping (boron) concentration and $[O_i]$ denotes the interstitial oxygen concentration. The factor two reflects the improvement of the bulk lifetime during the device fabrication process [18,23]. The intrinsic carrier lifetime limit given by Kerr and Cuevas [24] yields the bulk carrier lifetime for float zone (FZ) silicon as a reference material. Both, the SRV at the metallised and the SRV at the passivated area depend on the doping concentration. In this work we use parameterisations that reflect a thermal oxide passivated rear surface and LFCs formed on a $\sim 2 \mu\text{m}$ thick layer of evaporated Al. Moreover, we assume an emitter dark saturation current density of $J_{0e} = 250 \text{ fA/cm}^2$ and a second diode saturation current density of $J_{02} = 7 \text{ nA/cm}^2$. Recombination in the emitter and at the front surface reduces J_{SC} by 0.5 mA/cm^2 . The series resistance of the device involves the spreading resistance of the individual point contacts [25], which is proportional to the base resistivity ρ . The contact radius is $r = 45 \mu\text{m}$. In addition, a contribution of $0.5 \Omega\text{cm}^2$ is assumed for the lumped series resistance of the emitter and the front contact. The optical model represents a random pyramid textured front surface and a dielectric mirror at the rear surface. The front contact shades 5% of the device area.

Figure 6 shows the conversion efficiency plotted versus the base resistivity for a $150 \mu\text{m}$ thick device. The calculation applies the optimum rear surface metallisation fraction f for each resistivity value. Three types of material are considered. For high quality FZ material, our model predicts an optimum resistivity level of $\sim 0.5 \Omega\text{cm}$ enabling conversion efficiencies close to 20% for an industrial LFC PERC device. The low base resistivity reduces the series resistance losses, however, increased bulk and surface recombination start to overcompensate the gain in fill factor for even lower resistivity values. When recombination at boron-oxygen defect centres dominates in the bulk, higher resistivity values should be used. Depending on the interstitial oxygen concentration $[O_i]$, a resistivity between 1 and $2 \Omega\text{cm}$ should give the highest conversion efficiencies.

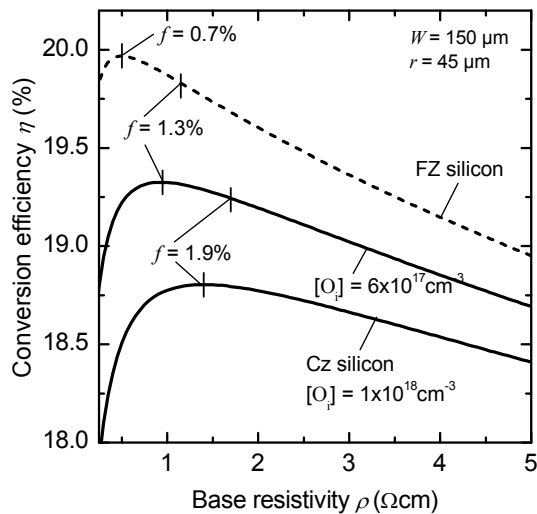


Figure 6: Analytically calculated efficiency of a 180 μm thick industrial p-type PERC device versus the base resistivity for intrinsically limit FZ silicon [24] and Cz silicon with different interstitial oxygen concentrations $[\text{O}_i]$ by Eq. (1). For each resistivity, the optimum metallisation fraction f is used. The contact radius is $r = 45 \mu\text{m}$.

5 SUMMARY

We use the SiNTO approach for the industrial fabrication of solar cells with local laser fired contacts. A stable efficiency of 18.4% is achieved for a SiNTO device fabricated from boron-doped Cz silicon. Compared to parallel processed Al-BSF solar cells, the efficiency gain is $\sim 0.5\%$ (absolute) for cells without and 0.8% (absolute) for cells with soldering pads. An IQE analysis reveals the superior surface passivation of SiNTO solar cells compared to the Al-BSF references. The EQE of the SiNTO solar cell exceeds that of the Al-BSF device down to bias illumination levels of 0.02 suns. To facilitate module interconnection, we introduce screen printed soldering pads and present a proof of concept for the combination of soldering pads with evaporated Al rear contacts. Finally, we apply a recently introduced analytical model to estimate the optimum base doping level for industrial, thermal oxide passivated LFC PERC devices fabricated from conventionally pulled Cz silicon. These calculations account for carrier recombination at boron-oxygen complexes and predict an optimum bulk resistivity between 1 and 2 Ωcm , depending on the interstitial oxygen concentration.

ACKNOWLEDGMENTS

We gratefully acknowledge fruitful discussions with the partners of the LFC-Cluster project and the support of the PV-TEC co-workers. This work is supported by the German Federal Ministry for the Environment, Nature Conservation and Reactor Safety under projects no. 0327572, 0329849B and 41V5674.

REFERENCES

- [1] A. W. Blakers, A. Wang, A. M. Milne *et al.*, *Appl. Phys. Lett.* **55** (1989) 1363.
- [2] O. Schultz, A. Mette, M. Hermle *et al.*, *Prog. Photovolt: Res. Appl.* **16** (2007) 317.
- [3] J. Zhao, A. Wang, and M. A. Green, *Prog. Photovolt: Res. Appl.* **7** (1999) 471.
- [4] D. Biro, S. Mack, A. Wolf *et al.*, *Proc. of the 34th IEEE Photovoltaic Specialists Conference* (2009) 1594.
- [5] A. Wolf, A. Walczak, S. Mack *et al.*, *Proc. of the 34th IEEE Photovoltaic Specialists Conference* (2009) 534.
- [6] D. Biro, R. Preu, S. W. Glunz *et al.*, *Proc. of the 21st European Photovoltaic Solar Energy Conference* (2006) 621.
- [7] E. Schneiderlöchner, R. Preu, R. Lüdemann *et al.*, *Prog. Photovolt: Res. Appl.* **10** (2002) 29.
- [8] A. Wolf, E. A. Wotke, A. Walczak *et al.*, *Proc. of the 35th IEEE Photovoltaic Specialists Conference* (2010) in press.
- [9] L. Gautero, M. Hofmann, J. Rentsch *et al.*, *Proceedings of the 34th IEEE Photovoltaic Specialists Conference* (2009) 1888.
- [10] J. F. Nekarda, M. Hörteis, F. Lottspeich *et al.*, *this conference*
- [11] P. A. Basore, *Proc. of the 23rd IEEE Photovoltaic Specialists Conference* (1993) 147.
- [12] M. P. Godlewski, C. R. Baraona, and H. W. Jr. Brandhorst, *Proc. of the 10th IEEE Photovoltaic Specialists Conference* (1973) 40.
- [13] S. W. Glunz, D. Biro, S. Rein *et al.*, *J. Appl. Phys.* **86** (1999) 683.
- [14] S. W. Glunz, A. B. Sproul, W. Warta *et al.*, *J. Appl. Phys.* **75** (1994) 1611.
- [15] A. G. Aberle, S. W. Glunz, A. W. Stephens *et al.*, *Prog. Photovolt: Res. Appl.* **2** (1994) 265.
- [16] S. Dauwe, L. Mittelstädt, A. Metz *et al.*, *Proceedings of the 17th European Photovoltaic Solar Energy Conference* (2001) 339.
- [17] S. Dauwe, L. Mittelstädt, A. Metz *et al.*, *Prog. Photovolt: Res. Appl.* **10** (2002) 271.
- [18] S. W. Glunz, S. Rein, J. Y. Lee *et al.*, *J. Appl. Phys.* **90** (2001) 2397.
- [19] J. Schmidt and K. Bothe, *Phys. Rev. B* **69** (2004) 0241071.
- [20] J. Schmidt and A. Cuevas, *J. Appl. Phys.* **86** (1999) 3175.
- [21] A. Wolf, D. Biro, J. Nekarda *et al.*, *J. Appl. Phys.* (accepted).
- [22] S. W. Glunz, J. Benick, D. Biro *et al.*, *Proc. of the 35th IEEE Photovoltaic Specialists Conference* (2010) in press.
- [23] K. Bothe, R. Sinton, and J. Schmidt, *Prog. Photovolt: Res. Appl.* **13** (2005) 287.
- [24] M. J. Kerr and A. Cuevas, *J. Appl. Phys.* **91** (2002) 2473.
- [25] R. H. Cox and H. Strack, *Solid-State Electron.* **10** (1967) 1213.